CHALMERS
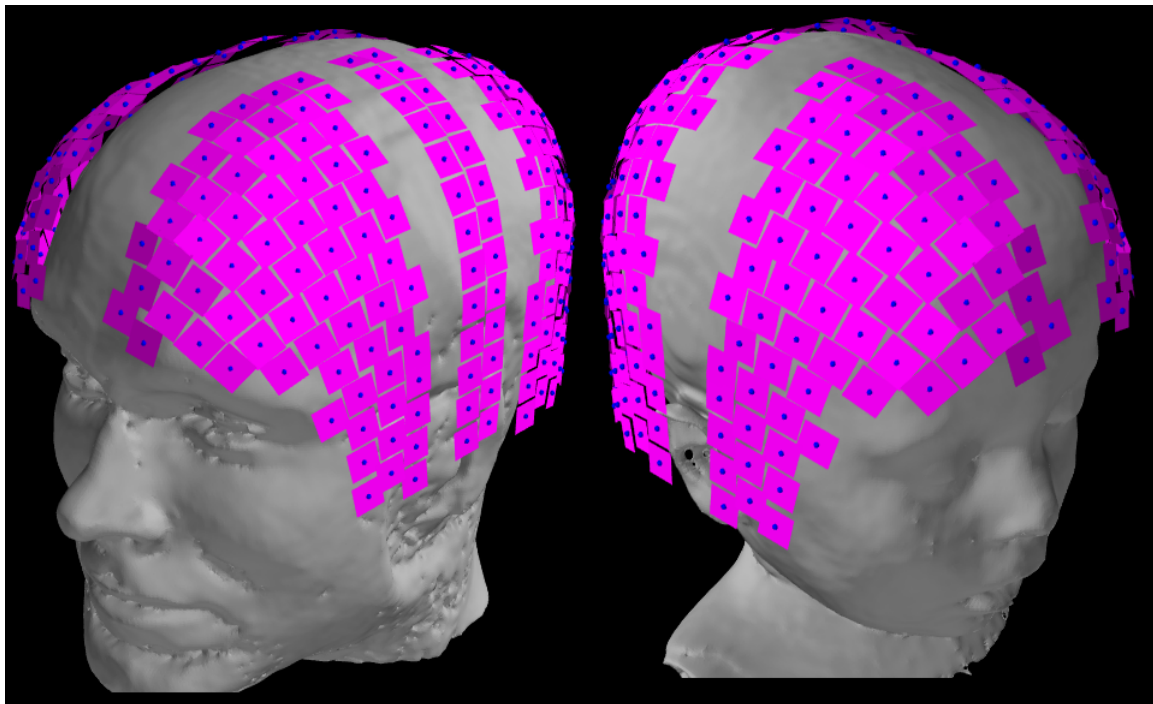### UNIVERSITY OF TECHNOLOGY

Optimizing design of on-scalp MEG systems
Master Thesis of Biomedical Engineering

FREDRIK BOLDIZAR

UNA SLIPAC

Acknowledgements

Abstract

Magnetoencephalography (MEG) is a non-invasive functional neuroimaging method. The advantages of MEG include high spatial and temporal resolutions which give precise, detailed information about the neural activity in the brain. State-of-the-art MEG systems use low critical temperature superconducting quantum interference device (low-Tc SQUID) sensors.

A major limitation for commercial MEG systems is related to the low-Tc sensors on which it relies: the need for an insulation space of $\sim 20\,\text{mm}$ between the sensors and the scalp of the subject increases the distance to the magnetic sources under study, i.e. neural currents in the brain. The insulation also decreases the flexibility of the system, so much so that anything other than a rigid helmet design is impractical. New advances in sensor technology such as high-Tc SQUIDs have made it possible to significantly reduce this insulation between each sensor and scalp, from a few cms down $\sim 1\,\text{mm}$. This allows for new MEG system designs that are flexible and more suitable for different head sizes and shapes. The aim of this project is to evaluate different configurations of on-scalp MEG sensor layouts that may be viable alternatives to conventional rigid helmet designs and can be more adaptable to individual subjects' head sizes and shapes.

The layouts were simulated on four different subjects, two primary and two secondary subjects. Simulations were done using MATLAB, python, and C, with software toolkits MNE-C and MNE-Python. Within this project, 8 different on-scalp layouts were simulated and compared to one another: the commercial Elekta Neuromag® system, and four on-scalp layouts previously desribed by Riaz et. al. The metrics used to evaluate the new MEG arrays were total information capacity (I_{tot}) and Spatial Information Density (SID) maps. Two different sensor noise levels were chosen, an optimistic one ($10\,\text{fT}/\sqrt{\text{Hz}}$) and a conservative one ($50\,\text{fT}/\sqrt{\text{Hz}}$). There were two approaches used when designing the new layouts: sets of similar layouts based on a simple geometrical shape and then distributed around the head, and segmentation of a helmet design into parts. These shapes were then covered with sensors using a Chebyshev net algorithm.

I_{tot} results indicate the Elekta system does not perform as well as most of the high-Tc layouts. This held true for both the optimistic and conservative noise levels. However, SID-maps provide evidence for the high-Tcs only being viable when using the optimistic sensor noise level of $10\,\text{fT}/\sqrt{\text{Hz}}$. Out of these results, the square-shaped cryostats and the segmented helmet were noteworthy, both of which ranked at the top according to all metrics.

Designing a practical and fully adaptable MEG sensor layout that is still viable performance-wise is a difficult task, and can be done in a number of ways. If using a large number of commonly shaped cryostats, then a square shape is preferred. When using the optimistic sensor noise level, a segmented helmet design was found to be most efficient regarding number of sensors and total information.

Keywords: *Magnetoencephalography, MEG, Superconducting quantum interference device, SQUID, brain mapping, High-Tc, functional neuroimaging*

Contents

1 Introduction

This section introduces the background of the thesis, followed by the Problem statement, Aim and Limitations set for the thesis.

1.1 Background

Magnetoencephalography (MEG) is a non-invasive functional neuroimaging method with high spatio- and temporal resolution, allowing very accurate measurement of brain activity in real time. It is used both for research and clinical purposes [1] [2]. The magnetic field generated by the brain is within the range of femto-Tesla to pico-Tesla, which is quite low compared to the Earth's magnetic field of $\sim 50\,\mu T$. Because of this, MEG systems require magnetically shielded rooms to operate and highly sensitive magnetic field detectors [3].

The combination of MEG and magnetic resonance imaging (MRI) is called magnetic source imaging and gives a large amount of information about the brain, both regarding structure and neural activity. The magnetic permeability of both the scalp and skull are almost the same as that of empty space, meaning that the strength of the field at a given point reduces by $1/r^3$ where r indicates distance from the source [3].

State-of-the-art commercial MEG systems use arrays of low critical-temperature (low-Tc) Superconducting Quantum Interference Devices (SQUIDs) due to their ability to combine high temporal resolution with low noise levels [1]. Compared to EEG systems (electroencephalography), the MEG signals pass through the scalp without any distortion. Another advantage with MEG over EEG is that MEG is more sensitive to superficial cortical activity, which is helpful when neocortical epilepsy is to be studied [3].

At the time of writing, the only commercial MEG system used in Sweden is the Elekta Neuromag® with a fixed-size low-Tc helmet. One of the biggest limitations of commercial low-Tc SQUID arrays is cooling down the sensors to the required operating temperature of ~4 Kelvin and shielding the patient from this cooling. Current systems use liquid helium to reach these extremely cold temperatures; helium is both expensive and requires a relatively thick insulation of $\sim 20\,mm$ between the subject's scalp and the sensor array. This insulation increases the distance to the neuromagnetic sources to which MEG is sensitive while also decreasing the flexibility of the system, so much so that anything other than a rigid helmet design is impractical [1].

New developments within magnetic sensor technology such as high critical temperature (high-Tc) SQUIDs, optically-pumped magnetometers (OPMs) and diamond nitrogen-vacancy center (N-V center) sensors have improved in sensitivity to the point where they are being considered as viable candidates for replacing the commercial low-Tc SQUIDs in use today [4]. Within this project, the sensor technology chosen for the simulations of on-scalp MEG arrays (i.e., sensors placed within $\sim 1\,mm$ mm of the scalp) is the high-Tc SQUID since the project is a continuation of work previously done at Medtech West. One advantage with high-Tc sensors is the use of liquid nitrogen cooling instead of the liquid helium used in the state-of-the-art MEG, and the subsequent new sensor operating temperature of ~77K [1]. This allows for a reduction in the stand-off distance between the subject and sensors, which in turn leads to an increase in signal magnitude. With this new sensor technology, it is possible to create more flexible MEG arrays which may lead to a flexible design that is adaptable to all head shapes and sizes.

MEG has become an important medical instrument. It contributes to clinical research within neurodevelopment and a better understanding of the brain. One advantage is that MEG systems have high spatial- and temporal resolution, where MEG tracks the structure of electrophysiological networks in real time [5]. Therefore, focus on developing a new generation of MEG systems such as on-scalp MEG is important within medical care.

With the advances in sensor technology mentioned above, a variety of new sensor arrays are made possible. By utilizing high-Tcs, in addition to reducing the subject-sensor stand-off, the reduction in size of the insulating walls around each sensor array could allow for a modular approach to layout designs. The adaptability to different subjects' head sizes and shapes allowed by such a design is something that current systems lack.

1.2   Problem statement

With the development of high-Tc SQUIDs, new flexible designs of MEG systems become possible. Some research has been done in the area of designing these layouts, but no general guidelines exist today.

1.3   Aim

The aim of the project is to evaluate different configurations of on-scalp MEG sensor layouts with the purpose of creating a viable alternative that is also adaptable to different subjects. By studying the many aspects that come into play during such design work, guidelines will be created which will potentially influence the future of on-scalp MEG development.

1.4   Limitations

- No metrics other than spatial information density maps and total information capacity will be considered when evaluating layouts.

- Only MNE-C and MNE-python will be used to simulate the different layouts, i.e. no other software will be used to get a "second opinion".

- All layouts will be placed onto subjects with the intent of maximum coverage, no neuroanatomical regions of interest will be taken into account.

- Only four subjects will be used for simulation of the various layouts, one adult and one child for primary designs and another adult and child for evaluation.

- Unlike the Elekta system, which uses both gradiometers and magnetometers, only magnetometers will be used for simulations. For fairness of comparison, the gradiometers of the Elekta system have been removed.

2   Theory

The theory part will include some brief explanation about MEG in general and the electromagnetic principles relevant to this work. Afterwards, the SQUIDs will be explained, followed by the theory behind source locations, and the metrics Total Information Capacity and Spatial Information Density maps.

2.1   Magnetoencephalography in brief and electromagnetic properties

Magnetoencephalography (MEG) is a functional neuroimaging or brain activity imaging technique that maps the neural activity that can help to understand the nervous system, and is used within medicine, neuroscience, and psychology [6]. An electrical current is always associated with a magnetic field perpendicular to the current direction, even the magnetic fields generated from the brain. At a cellular level, the MEG signals are caused by intracellular electric currents in the dendrites of pyramidal cells located in the cortical surface as illustrated in the images of figure 1. The cortical surface is the outer/surface layer of the brain.
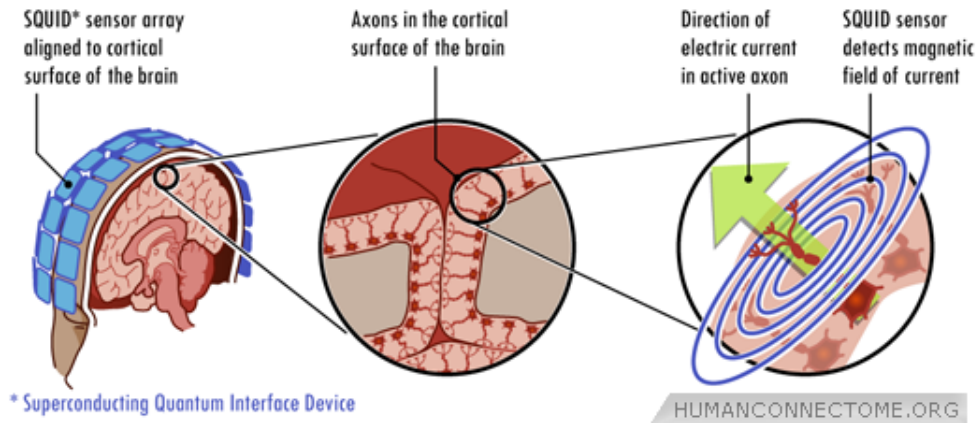

Figure 1: *SQUID measurement of magnetic fields from the brain* [7]

Changes in the brain's magnetic field are measured through highly sensitive sensors known as SQUIDs (Superconducting Quantum Interference Devices). The SQUIDs seen in the left image of figure 1 detect the very weak magnetic field outside the head. To be able to detect electrical activity from the dendrites, several pyramidal cells of the same orientation need to be activated simultaneously [8]. If the magnetic field is given by radial dipoles, i.e by currents perpendicular to the scalp surface, it can't be detected since the magnetic fields from radial dipoles do not reach outside the scalp [3].

Modern MEG systems have helmet-shaped arrays that employ more than 300 channels with 102 low critical-temperature SQUID sensors chips (each of which has 3 SQUIDs) placed around the surface [1]. The signals recorded by MEG directly reflect current flows generated by neurons within the brain. To be able to record these minute magnetic fields, the MEG system needs to be housed inside a magnetically shielded room to attenuate external noise. Also, an extremely cold environment, close to absolute zero, is required for SQUIDs to function. Since the magnetic field decays as $1/r^3$ where r is the distance from the source [3], i.e the cerebral cortex, the sensor placement should be as close to the source as possible to retrieve the best mapping.

One problem with modern MEG (Elekta) is to fit one helmet to different subjects, adults as well as children.
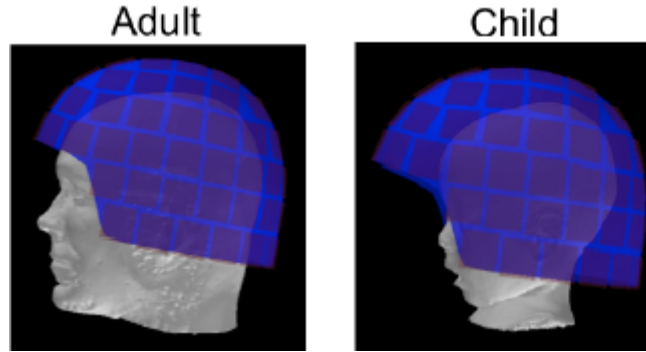
Figure 2: *The Elekta Neuromag system consisting of a rigid helmet* [4]

The Elekta MEG helmet is fixed to one size, although a system with a child-sized helmet also exists. Seen in figure 2, smaller head size contributes to a larger gap between the helmet and, e.g., the forehead if the subject rests his/her head at the back of the helmet. This means that the signals from the frontal areas would be not detected as strongly. This may be a problem for different adults as well, due to different head sizes and shapes. With the new developments in high-Tc technology, it is possible to create on-scalp helmets and other flexible layouts which are very close to the scalp, also making it possible to construct one adaptable setup for all head sizes.

Compared to the environmental magnetic interference, the magnetic fields generated from the brain are significantly smaller which in turn reduces the MEG signals signal-to-noise ratio (SNR). Many studies have shown that improvements in SNR contributes to improved spatial resolution [5]. MEG systems provide higher spatial- and temporal resolution as compared to EEG [3], which is advantageous since MEG allows better estimation of neural sources. Within digital images, spatial resolution refers to the number of independent pixel values per unit length [9], i.e how much detail can be resolved per unit of distance, and temporal resolution refers to frame rate, i.e how much detail can be resolved per unit of time [10].

There are different ways of evaluating the neuroimaging advantages of MEG when evaluating the performance of various MEG arrays. The two metrics total information capacity I_{tot} and spatial information density maps were evaluated for each sensor layout during analysis.

2.2 Superconducting Quantum Interference Devices (SQUIDs)

SQUIDs are used to detect ultra-sensitive and weak magnetic flux signals, based on superconductive loops interrupted by a pair of dual Josephson junctions [11]. SQUIDs are sensitive magnetometers that are capable of measuring magnetic fields at resolutions as low as 10^{-17} [12].

The word "Super-conducting" refers to superconductivity, which is a radical change of magnetic and electric properties in certain materials such as lead and mercury when reaching very low temperatures. The characteristics of superconducting materials are no electric resistance and a very large sensitivity to magnetic fields [13]. The transition from normal resistance to complete lack of resistance occurs at the transition temperature or critical temperature (Tc) that is material specific.

The main difference between low-Tc and high-Tc superconductors is their critical temperature. The low-Tc sensors require liquid helium cooling down to 4 K to be able to operate, whereas the high-Tc sensors need liquid nitrogen cooling to 77 K. The advantage with high-Tc is a reduction of the distance between the sensors and the scalp due to a decrease in the insulation required. Moving sensors closer to the head increases the MEG signal strength. Another advantage with high-Tc is that changing from liquid helium to liquid nitrogen significantly reduces operating costs [14] [1].

Due to the sensors cold environment, thermal insulation must be maintained between the scalp and detectors. The distance between source and sensors for low-Tc SQUIDs can be as low as 18 mm, but the typical scalp-to-sensor distance is between 20 and 30 mm [15]. But for high-Tc SQUIDs, the head to sensor standoff can be reduced to 1 mm. A drawback with high-Tc SQUIDs is that they suffer from higher thermal noise as compared to their low-Tc counterparts which may affect the brain mapping.

2.3 Source localization and forward model

One challenge posed by MEG is to accurately determine the source locations of the MEG signals based on measurement of the magnetic fields outside of the head. The location of activated neural sources must be estimated from the spatial distribution of the signal. To be able to compute the magnetic field distribution generated from the brain, the MEG data requires a mathematical model of the human head called a forward model [16].
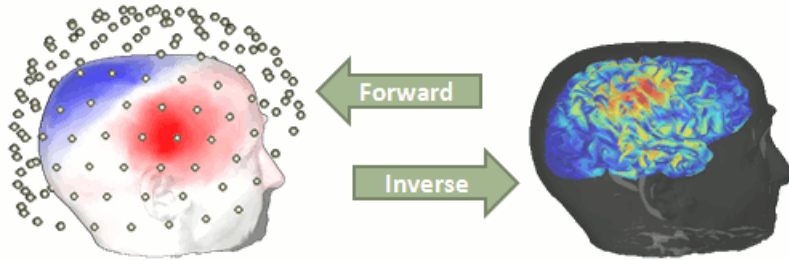

Figure 3: *Representation of the mathematical modelling to determine the source location, where the forward model is used*[17].

The forward model represents the reconstruction of the electrical activity from the neural sources of MEG data, where the model parameters (source location, right image in figure 3) are known and the data (the magnetic field from a distance, left image in figure 3) is to be estimated. The forward model is a matrix with the size [number of sensors] × [number of sources] [17].

2.4 Total information capacity

The SQUID sensors are noisy channels which convey the information from the source of the field, where the total information, I_{tot}, conveyed by the entire MEG array allows comparison to other magnetometer arrays without reference to a specific source model. The information gained per one sample can be determined through Shannon's theory of communication [18]:

$$I = \frac{1}{2}\log_2(P+1) \tag{1}$$

where I is information capacity measured in bits and P is the power signal-to-noise ratio (SNR) that depends on how well the source is coupled to the sensor, for both high-Tc and low-Tc SQUIDs [14] [8]. The calculation of *total* information conveyed by the entire array is equal to the summation of all the orthogonalized and independent channels of the array,

$$I_{tot} = \frac{1}{2}\sum_k \log_2(P'_k+1) \tag{2}$$

where P'_k is the SNR of the k-th *orthogonalized* channel, and the information in each channel must be independent. To establish the equation of P'_k, the following definition is needed:

- Assume that the generations of neural current dipoles obeys normal distribution in each non-radial direction:

$$J_{\theta,\phi} \sim \mathcal{N}(0, \sigma_{signal}^2) \tag{3}$$

  where $J_{\theta,\phi}$ is the sub-components of the total neural currents $\bar{J}(r)$ in spherical coordinates.

- The lead field (also known as the forward model or the gain matrix [17]) of a sensor, which is the coupling between the sensors and the magnetic field generated by currents inside the brain, and describes the sensitivity distribution of the k-th magnetometer

$$S = \int_V \bar{L}(r) \cdot \bar{J}(r)dr = \sigma_{signal}^2 \int_V |\bar{L}(r)|dr \tag{4}$$

  where S is the sensor recorded magnetic field strength and $L(r)$ is the lead field. The second equality is given by equation (3)

- Assume normally distributed noise for each channel,

$$N_k \sim \mathcal{N}(0, \sigma_{noise}^2) \tag{5}$$

- Total power SNR is equal to

$$P = \frac{S^2}{N^2} = \frac{\sigma_{signal}^2}{N^2} \Big(\int_V |(\bar{L}(r)|dr \Big)^2 \tag{6}$$

  where the second equality is given by equation (4).

The sensors of multi-channel MEG systems can receive signals from the same sources, i.e. the lead field of the sensors overlap and makes the channels dependent. Therefore, the channels are re-created as independent and orthogonalized channels to gain P_k' and then I_{tot}. The inner-product of the lead field for each pair of sensors is calculated from the forward solution/gain matrix G [19] (mathematical modelling estimation, introduced in chapter 2.3)

$$\Lambda_{ij} = \int_V \bar{L}_i(r) \cdot \bar{L}_j(r)dr = GG^T \tag{7}$$

where the Λ is decomposed via singular-value decomposition to orthogonalize the channels:
$\Lambda = U\bar{\lambda}U^T$ where $\bar{\lambda} = \text{diag}(\lambda_1, \lambda_2, \dots \lambda_m)$. U represents a matrix containing the eigenvectors of Λ and U^T it's transpose. λ_k is the eigenvalues of the lead field matrix Λ. The independent k-th channel can be determine by the orthogonalized lead fields:

$$\bar{L}_k' = U^T \bar{L}_k \tag{8}$$

where the apostrophe indicates on orthogonalized channels. The power signal-to-noise ratio for an orthogonalized channel k can be determined from equation (6) [20]

$$P_k' = \frac{\sigma_{signal}^2}{\sigma_{noise,k}'^2} ||\bar{L}_k'||^2 \tag{9}$$

where $\sigma_{noise,k}'^2 = \sum_j (m_{ij}\sigma_{noise,j})^2$ and the matrix $[M]_{i,j} = m_{ij}$ can be chosen as $M = U^T$ because then $\Lambda' = U^T\Lambda U = (U^TU)\bar{\lambda}(U^TU) = \bar{\lambda} = \text{diag}(\lambda_1, \lambda_2, \dots \lambda_m)$ [18]. From this and equations (7), (8) and (9), the orthogonalized SNR from the k-th channel P_k' is calculated as

$$P_k' = \frac{\sigma_{signal}^2 \lambda_k}{\sum_j (U_{kj}\sigma_{noise\,j}^2)^2} \tag{10}$$

6

where P'_k is inserted in equation (2) to gain the total information I_{tot} for the entire array.

The advantage with total information capacity is that I_{tot} quantifies aspects such as sensor distances to the source, sensor configuration, SNR and sensor type [21]. One disadvantage with total information is that the knowledge of spatial distribution is lost, i.e there is no way to know where the information is coming from. The lack of spatial distribution information depends on how the independent and orthogonalized channels are made and how they sample the brain [4].

2.5 Spatial information density maps

Due to the lack of spatial (voxel- or patch wise) variation in I_{tot}, spatial information density maps (SID-maps) are introduced as an additional metric that combines information capacity with spatial distribution. Looking in a single patch/source in the brain, the SID value is

$$SID_{patch} = \frac{1}{2} \log \Big(\frac{\sigma_{signal}^2 \lambda_{k,patch}}{\sum_k (U_{k,patch} \sigma_{noise}^2)^2} + 1 \Big) \tag{11}$$

λ_{patch} represents the eigenvalues and U_{patch} are the eigenvectors of the lead field matrix Λ_{patch} for a single source of the head surface. Shown in chapter 2.4, the lead field matrix of a single patch can be determined from the forward solution/gain matrix G for a single patch [4]

$$\Lambda_{patch} = G_{patch} \cdot G_{patch}^T \tag{12}$$

Summarizing all the patches, the average SID of the entire brain is then

$$SID_{avg} = \frac{1}{N} \sum_{i=1}^{N} SID_{patch,i} \tag{13}$$

3   Method

Below are the details of the various materials used, the creation of different cryostat and sensor layouts as well as the simulation pipeline.

3.1   Software toolkits

This thesis work was done using MATLAB, python and some C programming. It is reliant on the software toolkits MNE-C and MNE-Python.

3.2   Anatomical model

Four T1-weighted MRIs were used in this study: a 35 year-old male, a 2 year-old child, a 30-year-old female and a second 2-year-old child. The adult MRIs are of two of the staff at MedTechWest, while the child MRIs are taken from the open repository brain-development.org. The details of each subject can be seen in table 1.

Table 1: Subject MRI data

Subject	Cortical Surface Area	Number of sources
Adult	94 030 mm^2	156 176
Child	77 637 mm^2	127 931
Adult2	88 644 mm^2	137 248
Child2	85 896 mm^2	143 721

As can be seen above, the surface areas and number of sources for the first two subjects differ the most. The assumption is done that by using these two widely different subjects, the adaptability with regards to different head shapes of each layout can be included to some extent in the result.

3.3   Sensor specifications

The sensors used in the new simulated layouts are high-Tc SQUID magnetometers with a pickup loop of size $8\,\text{mm} \times 8\,\text{mm}$, a total size of $11\,\text{mm} \times 11\,\text{mm}$ and a sensor-to-sensor gap of $0.5\,\text{mm}$. These same sensor specifications are used in the high-Tc simulations by Riaz et. al [4], which are compared with in the result. All high-Tc sensors are simulated at two different noise levels: an optimistic noise level of $10\,\text{fT}/\sqrt{\text{Hz}}$ and a conservative noise level of $50\,\text{fT}/\sqrt{\text{Hz}}$. These noise levels are based on earlier studies done with high-Tc SQUIDs [22] [23].

The only exception to these sensor specifications is the Elekta Neuromag® system, where the MNE-generated model of the system is used. There, each sensor is a low-Tc magnetometer with a pickup loop of size $25.8\,\text{mm} \times 25.8\,\text{mm}$. The noise level of the sensors used in the Elekta system is $3\,\text{fT}/\sqrt{\text{Hz}}$.

As mentioned earlier in this section only magnetometers are used in the simulations, as opposed to the magnetometers and gradiometers of the Elekta system. Gradiometers have better noise reduction [3], but are also more complicated to simulate. To simplify and speed up the calculations, they are not included in the simulated layouts. In order to keep the comparison fair, the gradiometers are removed from the Elekta sensor array as well.

3.4   Forward model

The gain matrix G for the forward solution was calculated using a single layer model Boundary Element Method (BEM) with a conductivity of 0.33 S/m in MNE-python. For both high- and low- Tc SQUIDs,

the output of the sensors was calculated by integrating the magnetic flux on 16 points covering the pickup coil loops [4].

3.5 Layout selection

In this section, all layout designs and the idea behind them being evaluated is explained. The main focus of the design work during the thesis was to create adaptable designs and as a result, every layout proposed is modular.

3.5.1 Optimizing geometrical layouts - Packing problems

Most of the on-scalp MEG arrays proposed in this report contain geometrically shaped cryostats, where each cryostat contains a number of densely packed sensors (also referred to as channels). A cryostat is a housing for the sensors that allows for coolant to be pumped through it. Therefore, each cryostat requires a layer of insulation around it which further increases its size. A cryostat's shape can vary greatly, whereas the sensors are always square shaped. The idea is that packing several sensors into movable cryostats will result in increased flexibility while still performing well enough to be able to compete with state-of-the-art designs.

Within this project, the cryostat geometries tested were circular-, hexagonal- and square-shaped. This lead to three separate packing problems, see Figure 4.
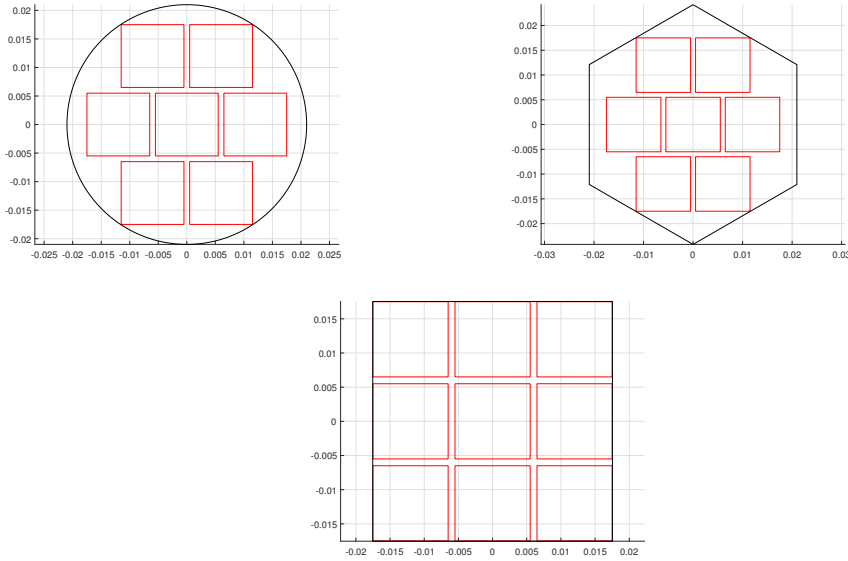

Figure 4: *Illustration of the packing problem solutions used for different shapes*

The red marked squares in figure 4 represent the SQUID sensors, and the three black outlines represent cryostats. All sensors are a fixed $11\,\text{mm} \times 11\,\text{mm}$ but the number of sensors/the size of the cryostat is variable. The goal is to maximize the number of sensors inside the cryostat, i.e the difference between the total area of the cryostat and the area of all sensors summarized should be as small as possible. This was calculated by creating a script to calculate the number of sensors possible to fit into a shape (circle, square or hexagonal) based on the radius of that shape, then increasing the radius in small increments and noting each time a larger sensor amount was fitted.

As mentioned earlier in this section, all cryostats require an insulating wall around them. This has

been approximated to an increase in 6 mm (for high-Tcs of 77 K) on the shortest radius of each shape. In order to fit more closely to the general shape of the scalp, each sensor array is also offset into a bowl-like shape. This is done by projecting the 2D arrays such as those seen in Figure 4 onto a 3D sphere. The radius of the sphere was a fixed 8 mm.

According to figure 4, the square-shaped cryostat has the least empty space compared to the circular and hexagonal layouts since the sensors are square-shaped. The reason for introducing the other two geometries is another packing problem, namely the placement of cryostats around the head of the subject. On the one hand, we want to minimize the empty space by inserting as many sensors as possible. On the other hand, increasing the size of cryostats makes it harder to fit them tightly around a subjects head.

3.5.2 Choosing cryostat size

The radius of each cryostat shape was increased in small increments of 0.01 mm and a note was made each time more sensors were added. For each noted radius, the area usage (including cryostat walls) was calculated. The results can be seen in table 2.

Table 2: *The minimal radius (including cryostat walls) to fit each sensor amount, calculated for each cryostat shape and sorted by radius size.*

Circular		
# sensors	*Radius (mm)*	*Area usage (%)*
12	3.22	38
14	3.54	37
15	3.61	39
17	3.77	40
18	3.93	39
21	4.04	44

Square		
# sensors	*Radius (mm)*	*Area usage (%)*
4	2.23	49
9	3.08	58
16	3.93	63
25	4.78	66
36	5.63	69

Hexagonal		
# sensors	*Radius (mm)*	*Area usage (%)*
8	3.27	43
10	3.32	52
12	3.62	51
14	3.87	52
16	4.01	55
17	4.06	56

The area usage is calculated as the summarized area of all sensors in one cryostat, divided by the total area of the cryostat. As mentioned before, the empty space between the sensors and the cryostat should be as small a factor as possible, i.e the larger area usage, the better. Seen in table 2, it is obvious that area usage increases with cryostat size, but there is an upper limit to cryostat size as well, especially to fit onto smaller head sizes. Hence, increasing the number of sensors/channels in one cryostat above a certain amount is not beneficial since it tends towards a more rigid design while not fitting closely to the curvature of the head.

The circled entries in table 2 are the layouts chosen for simulation. The goal was to have a variety

of cryostat sizes in an attempt to find an optimal size-to-flexibility ratio while also keeping a relatively large area usage. For instance, the 12-channel circular layout radius is 3.22 mm with an area coverage of 38% compared to the 14-channel circular where the radius increase to 3.54 mm but the area usage decreases to 37%. One can see in table 2 that the best area usage of 69% is the 36-channel square layout, but the large size of the cryostat (5.63 mm radius) makes it impractical. From the chosen layouts, the largest one is the 17-channel hexagonal layout with a radius of 4.06 mm. Through testing it was found that a larger radius than that gave the cryostat a shape too large and general to fit well onto both an adult and a child.

3.5.3 Segmented helmet layout

When designing the segmented helmet, only the two primary subjects adult and child were used. Its layout can be seen in figure 5. The helmet contains six parts in total, with only the front and back parts being used for the child.
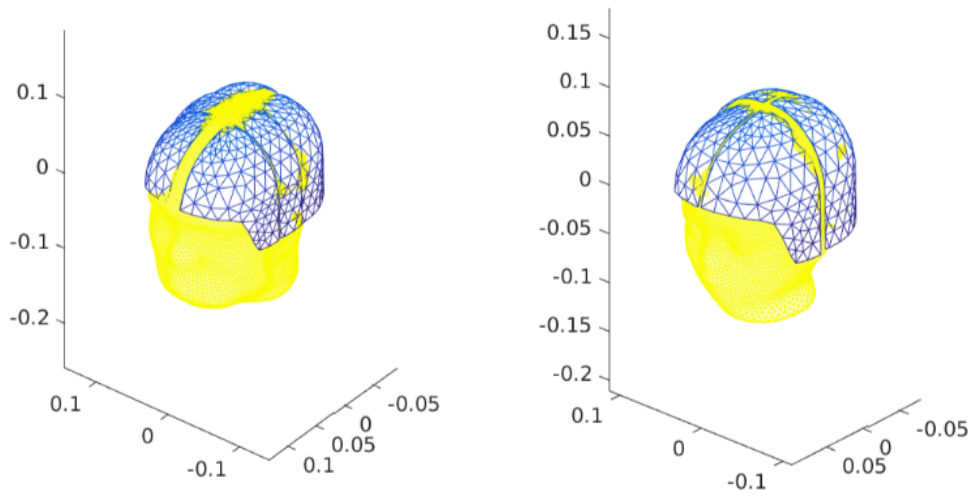

Figure 5: *The segmented helmet placed onto an adult and child head, including cryostat walls. Adult to the left, child to the right.*

Each segment is a scaled slice of the Elekta helmet, the shape of which is very well adapted to a large percentage of adult head-shapes. Sensors have been distributed across the surface of each segment using Chebyshev iteration as proposed by Popov et. al. [24], taking into account cryostat walls between each segment. The size of the front and back segments have been set to fit the child's head, while the middle segments are the minimum width to fit two rows of sensors.

3.5.4 List of simulated layouts

The layouts simulated during this project are as follows:

1. **Circular** - 21-channel, 17-channel and 12-channel cryostats.

2. **Square** - 16-channel and 9-channel cryostats.

3. **Hexagonal** - 17-channel and 10-channel cryostats.

4. **6-piece Segmented Helmet** - 6 pieces used for the adult, 4 pieces used for the child.

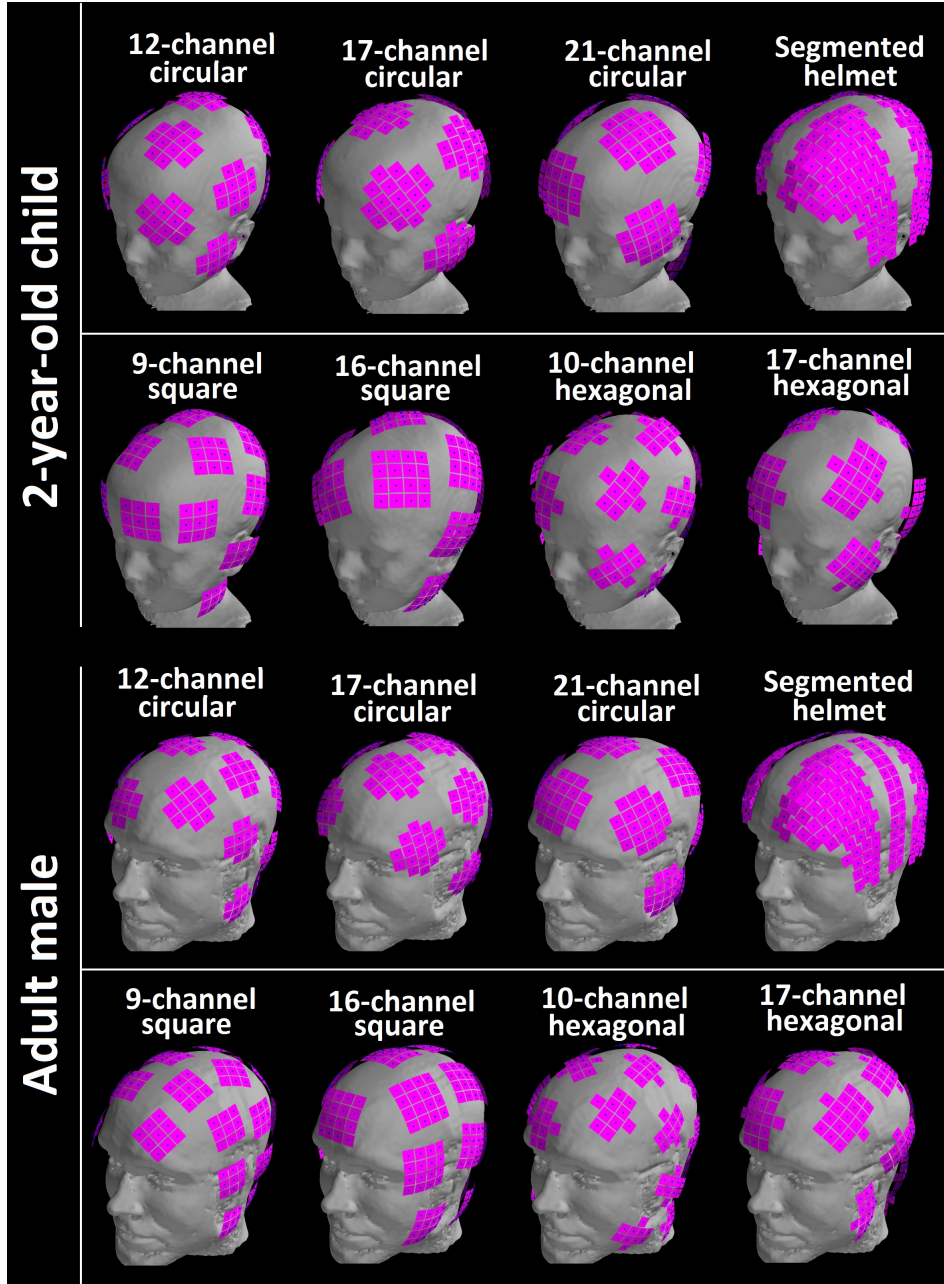These layouts can be seen in figure 6.

Figure 6: *All newly devised sensor layouts and their placements for main the subjects*

Additionally, the layouts first designed by Riaz et. al [4] were simulated for comparison, see figure 7.
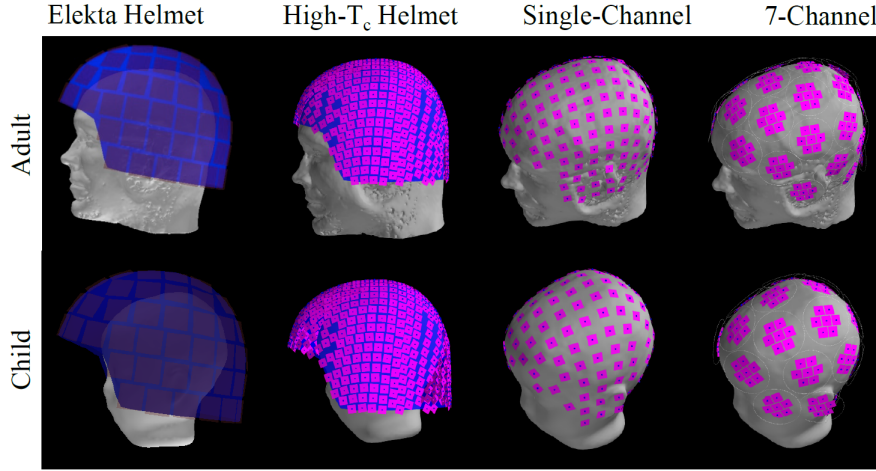
Figure 7: *The additional layouts discussed in the paper by Riaz et. al, illustrated on both child and adult heads* [4]

3.5.5 Cryostat placement

For placement of the cryostats, the evaluated designs can be divided into two major categories.

- Geometrically shaped cryostats: sensors are packed inside a geometrically shaped(i.e square, circular or hexagonal) cryostat, where all cryostats of one layout are of the same size.

- Irregularly shaped cryostats: sensors are placed densely across one or several irregular surfaces (i.e not a basic geometrical shape) which are shaped to fit to a general shape of the head.

The geometrically shaped cryostats are placed by manually selecting a point on the scalp. The normal of the scalp at that point is used to align the cryostat to the surface. A "shadow" of the cryostats outline is cast onto the subject which is used to ensure that cryostats do not overlap. The angle of each cryostat is tweaked to align it correctly at that particular point on the scalp. Finally, cryostats are moved so that all sensors are within 1 mm-1.5 mm from the surface. For the square and hexagonal layouts, each array can also be manually rotated to allow them to be placed as closely as possible to each other.

The placement of the segmented helmet cryostats was very simple (see figure 5). Each piece is placed manually and then automatically adjusted so that a) each sensor is outside the 1 mm minimum distance and b) the topmost sensor is no further than 2mm from the scalp. No rotation is involved for these placements.

The other irregularly shaped cryostat designs (single-channel, Elekta helmet, high-Tc MEG helmet) are those first done by Riaz et. al. [4]. Both the high-Tc helmet and the Elekta helmet were placed through use of the device- to subject-space transform as detailed in chapter 3.6.1. The single-channel and high-Tc helmet layouts were created using chebyshev iteration. The single-channel layout is distributed across the scalp of each subject, while the high-Tc helmet layout is distributed across a helmet model. The Elekta helmet model included all sensor locations when received. For more information, see the paper by Riaz et. al..

3.6 The simulation pipeline

The simulation pipeline used for the project is similar to the one used previously by Riaz et. al. at MedTechWest [4]. Additions include code to generate sensor locations along a subjects head in hexagonal, circular and square shapes of any size as well as creation and placement of the segmented helmet.

The pipeline can be divided into two parts: The subject pipeline and the sensor pipeline.

3.6.1   The subject pipeline

These operations are done once for each subject.

1. **Obtain .fif data of the desired subject** - These are generated during any MEG examination.

2. **Create subject- to device-space transform** - The data of the subject model and the data of the device model might not be centered the same in 3D-space. To correct this, a transform is created through manual selection of cephalometric landmarks using the mne_analyze command of the MNE-C toolbox.

3. **Generate the subject's source space** - In order to estimate a response from the sensor arrays, electrical dipoles are simulated across the surface of the brain. The resolution (i.e. the distance between each dipole) is set to $2\,\mathrm{mm}$ for all simulations.

3.6.2   The sensor array pipeline

These operations are done (at least) once for each subject and sensor array.

1. **Place sensor (array) locations around head** - This step varies depending on what type of array is used.

2. **Assign information to each sensor** - In order to use the MNE toolboxes, the sensor data needs to be set according to a certain information framework. The only significant part of this framework in our case is the type of sensor used, i.e. magnetometers.

3. **Calculate the forward solution/gain matrix** - The gain matrix contains information between the source space (see the subject pipeline above) and each sensor. It is the calculation of how much each dipole source is registered in each sensor.

4. **Calculate SIDmaps and Itot** - See the theory section 2.5 above for detailed explanations about these metrics.

4   Result

Below are the results of simulations performed on the layouts designed during this thesis. The majority of this chapter describes the evaluation of all layouts on the adult male subject and the 2-year-old child subject due to them being the largest and smallest subjects as can be seen in table 1. From the resulting figures, the four overall best performing layouts are chosen and evaluated on the other two subjects.

4.1   Final layouts

8 different layouts were simulated during this project, which were then compared to the commercial Elekta system and the high-Tc simulations first done by Riaz et. al [4]. The table below shows the summarized array parameters determined from these simulations.

Table 3: *Parameters for each layout. The first three simulations below the double line was simulated by Riaz et. al. [4] and the last layout (Elekta) is the commercial MEG system.*

	Average standoff from scalp (mm) *Male Adult/2-year-old Child*	Total number of sensors *Male Adult/2-year-old Child*
12-channel circular	2.8/2.6	264/204
17-channel circular	3.3/3.5	272/187
21-channel circular	3.6/4.5	294/231
9-channel square	2.5/2.5	297/216
16-channel square	3.6/3.6	352/224
10-channel hexagonal	3.3/2.9	260/190
17-channel hexagonal	5.5/4.6	289/204
Segmented helmet	4.6/4.7	376/324
High-Tc helmet	9.6/21.2	631/631
Single channel	1/1	214/161
7-channel	1.9/1.8	210/161
Elekta	28.9/40.2	102/102

Shown in table 3 is the average standoff between scalp surface and the sensors in millimeters as well as the total number of sensors for each layout and both subjects. The number of sensors for Elekta and high-Tc helmet layouts are always fixed due to being distributed on a fixed-size helmet, whereas the number of sensors for the other layouts vary based on the number of cryostats that can be placed for different head sizes. The average standoff distance is always fixed for single channel since the layout is distributed evenly (i.e a fully flexible design) around the head where each sensor is placed 1 mm from the scalp. The red marked digits highlight the best values of all the MEG arrays that contribute most to gained information (for our simulations and from previously done simulations by Riaz), i.e. a high number of sensors and a low average standoff distance.

For our simulations sampled on both the adult and the child, the segmented helmet has the highest number of sensors with 376 and 324 respectively, placed around the head. But the high-Tc helmet layout has the highest number of sensors by far, 632. Notice the large average standoff for the high-Tc helmet array placed on the child, this is due to the large gap between the forehead and the rigid helmet. For our simulations, the smallest average standoff is the 9-channel square layout with a distance of 2.5 mm for both subjects, whereas the overall minor standoff is from the single channel layout with average distance of 1 mm as expected. Notice that the average standoff distance for the segmented helmet is high for both subjects, but also has a very high number of sensors compared to the other modular layouts.

As can been seen in table 3, increasing the size of the cryostat also increases the average standoff distance (compare for example the 12-channel circular to the 21-channel circular), which based on theory is

as expected due to smaller cryostats having a shorter distance between the furthest and the closest sensors. Small cryostats allow the sensors to be placed closer to the head since no head surface is completely spherical. The total number of sensors also increases when increasing the size of a cryostat, with one exception for the 17-channel circular placed on the child.

The layout with the highest number of sensors or the smallest average standoff might not give the best results when evaluating the total information or the SID-maps. Other parameters such as signal-to-noise ratio, how well the cryostats fit different surfaces and how much empty space is between the cryostats also influence the final result.

4.2   Total information capacity

The total information conveyed from the source is measured in bits and plotted over the orthogonalized channels. The presented plots below use the conservative high-Tc SQUID noise level of $50\,\mathrm{fT}/\sqrt{\mathrm{Hz}}$ for all new high-Tc MEG layouts when calculating and evaluating total information capacity (I_{tot} from the Theory section, chapter 2.4). For the commercial Elekta system the noise level is fixed at $3\,\mathrm{fT}/\sqrt{\mathrm{Hz}}$.
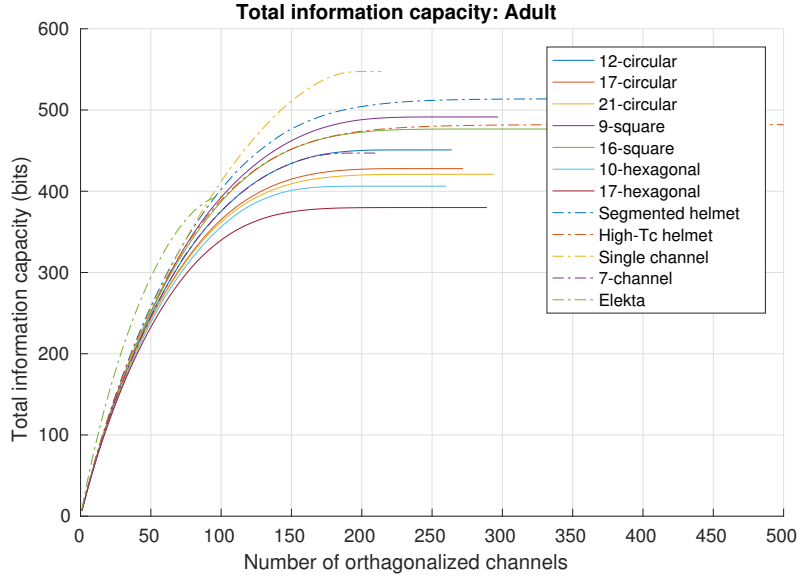

Figure 8: *Cumulative sum of total information capacity for all the on-scalp layouts and the commercial Elekta system, sampled on the adult with a noise level of* $50\,\mathrm{fT}/\sqrt{\mathrm{Hz}}$.
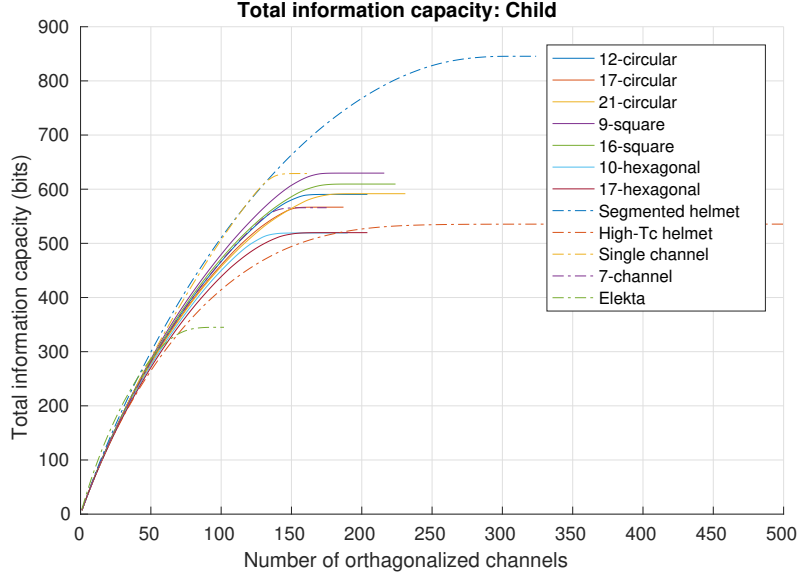
Figure 9: *Cumulative sum of total information capacity for all the on-scalp layouts and the commercial Elekta system, sampled on the child with a noise level of $50\,\mathrm{fT}/\sqrt{\mathrm{Hz}}$.*

For all the layouts on both subjects, the cumulative information flattens out and doesn't increase significantly for a number of orthogonalized channels, seen in figures 8 and 9. For the adult case, looking at the beginning of the slope (number of orthogonalized channels are low), the Elekta system (green dashed line) increases faster than all the high-Tc SQUID arrays and does not flatten out until near the end (stops at ~ 100 channels) unlike the high-Tc layouts. But for the child case, the curves are similar for all the layouts.

For the adult, figure 8, the single channel collects the most information, with the segmented helmet coming shortly thereafter. Other high-Tc layouts that showed interesting results for the adult are the square-shaped cryostats, both the 9-channel (purple line) and 16-channel (green line). The square cryostats also performed well for the child case, whereas the most information by far was gathered by the segmented helmet. As expected, since the segmented helmet was made to fit the child perfectly, (see figure 6).

Even though the high-Tc layouts were chosen to have a high sensor noise level equal to $50\,\mathrm{fT}/\sqrt{\mathrm{Hz}}$ compared to the Elekta's noise level of $3\,\mathrm{fT}/\sqrt{\mathrm{Hz}}$, the majority of the simulated high-Tc layouts gather more information than the commercial Elekta system for both subjects. As can been seen in both figures above, the worst performing cryostat geometry when analyzing the total information capacity was the hexagonal shaped cryostats, where the 17-channel hexagonal shaped cryostat is inferior than the Elekta system for the adult case.

The table below shows the maximal information gained from all the layouts, using both the conservative high-Tc noise level equal to $50\,\mathrm{fT}/\sqrt{\mathrm{Hz}}$ and the optimistic noise level equal to $10\,\mathrm{fT}/\sqrt{\mathrm{Hz}}$, for both subjects.

Table 4: *Maximal information capacity, all layouts sampled on both the adult and the child for both the conservative and optimistic sensor noise level.*

	Adult		Child	
	$\sigma_{noise} =$ $50\,\mathrm{fT}/\sqrt{\mathrm{Hz}}$	$\sigma_{noise} =$ $10\,\mathrm{fT}/\sqrt{\mathrm{Hz}}$	$\sigma_{noise} =$ $50\,\mathrm{fT}/\sqrt{\mathrm{Hz}}$	$\sigma_{noise} =$ $10\,\mathrm{fT}/\sqrt{\mathrm{Hz}}$
12-channel circular	450.9	875.7	590.4	969.5
17-channel circular	427.9	844.4	566.8	929.5
21-channel circular	420.9	836.0	591.7	1006.9
9-channel square	491.5	958.4	629.7	1030.0
16-channel square	476.6	944.7	609.5	1016.9
10-channel hexagonal	406.3	780.5	519.1	848.5
17-channel hexagonal	379.9	755.3	519.8	879.8
Segmented Helmet	513.7	1039.1	845.5	1493.6
high-Tc helmet	482.0	998.8	535.5	1054.5
single-Channel	547.5	984.5	629.0	968.3
7-channel	447.0	845.7	565.8	909.9
Elekta $(\sigma_{noise} = 3\,\mathrm{fT}/\sqrt{\mathrm{Hz}})$	393.4		345.0	

For the adult, one can see in table 4 that larger cryostats experience a decrease in the total information gained from the source (for instance the 9-channel square has $I_{tot} = 491.5$ and 16-channel squared has $I_{tot} = 476.6$ for noise level equal to 50). This is not true for the child case, for instance the 21-channel circular layout has higher I_{tot} value than the 12-channel circular layout. The reason for this pattern is that the head shape of this specific child is almost spherical, whereas the adult is not. The curvature of all cryostats are the same, which means that a larger cryostat should be a worse fit to a non-spherical surface than the smaller cryostats.

The circled layouts in table 4 represents the four simulated high-Tc layouts that had the largest I_{tot} for both subjects with the two different noise levels, which was the segmented helmet, the two square-shaped cryostat layouts and the circular 12-channel. These layouts were simulated on two other subjects, one female adult and another child, as can be seen below in chapter 4.4.

One can see that the high-Tc helmet helmet and the single channel gain more information than the 12-channel circular shaped for the adult. The reason for excluding these is that the single-channel is not practical and the high-Tc helmet layout performed poorly for the child compared to the other layouts. That the 12-channel circular layout gained more information than the 7-channel circular is of interest, for both subjects with both noise levels, which is the reason for including it in the final layouts to simulate on the other two subjects. Notice that the 21-channel circular actually has better performance than the 12-channel circular layout for the child, but 12-channel had a better overall performance.

Worth mentioning is that different noise levels influence the performance of the layouts non-linearly. Looking at the high-Tc helmet for the child (last two columns in table 4), it is ranked as the second best layout for the optimistic noise level ($10\,\mathrm{fT}/\sqrt{\mathrm{Hz}}$), but for the conservative noise level it comes in at 9th. This is due to the number of sensors. There are 631 sensors in the high-Tc helmet layout [4], which is a lot compared to the other layouts (see table 3). Since increasing the noise has an immediate effect on the SNR of each sensor, and the signal is mainly reliant on distance, decreasing the noise effectively increases the detection range of each sensor.

4.2.1   Power Signal-to-Noise Ratio

Seen from the result of total information capacity (figure 8 and 9), the last number of orthogonalized channels don't add to the total information for the high-Tc layouts. For all MEG arrays, the power SNR, measured in decibel, over orthogonalized channels (P'_k in the Theory section, chapter 2.4) with conservative high-Tc SQUID noise level equal to $50\,\mathrm{fT}/\sqrt{\mathrm{Hz}}$ is evaluated to be able to determine the number of orthogonalized channels that don't significantly add to the total information. This is defined as having an SNR lower than one (below $0\,\mathrm{dB}$), where the SNR is calculated for both subjects.
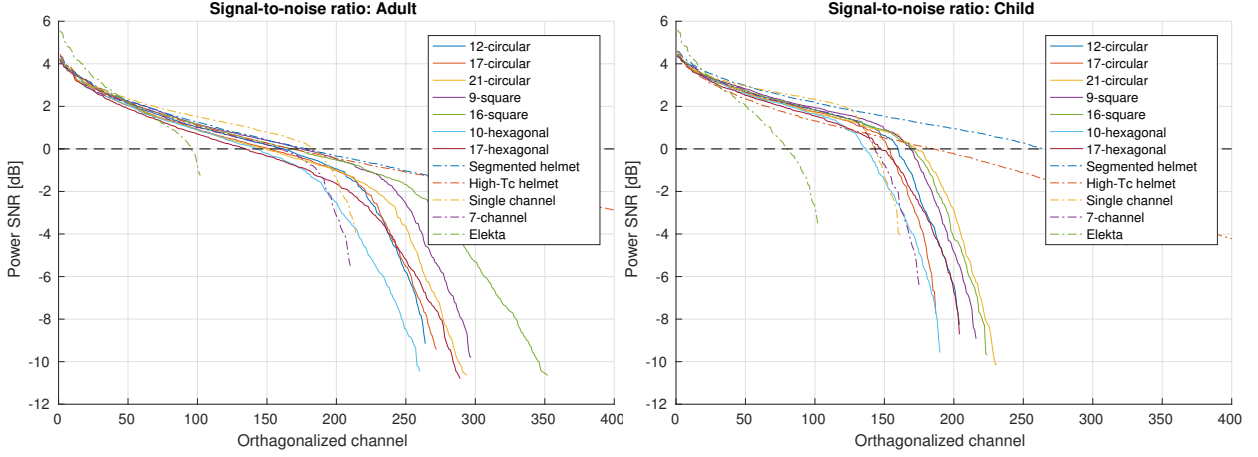

Figure 10: *Signal-to-noise ratio using the conservative sensor noise level, left figure sampled on the adult and right figure sampled on the child.*

The black dashed line at zero in Figure 10 is a reference line, where values above this line is the number of channels that achieves SNR > 1. For the Elekta system (green dashed line) for the both Adult and Child, the number of unnecessary orthogonal channels (channels that fall below the black dashed line) is quite small compared to the high-Tc simulations.

4.3   Spatial information density (SID)

Within the SID subsection, the average SID values are calculated and the simulated SID-maps are presented below, for each layout sampled on both primary subjects.

4.3.1   SID average

The average of SID values over the source space is an additional metric to I_{tot} and is measured in bits per source. The SID average of each layout is calculated and plotted for each subject. The SID average of on-scalp layouts is a function of sensor noise from 1 to $50\,\mathrm{fT}/\sqrt{\mathrm{Hz}}$. The SID average of the Elekta system is 1.5 and 1.6 bits/source for the adult and child respectively, represented by a horizontal dashed reference line. For the Elekta helmet the noise level is a fixed $3\,\mathrm{fT}/\sqrt{\mathrm{Hz}}$.
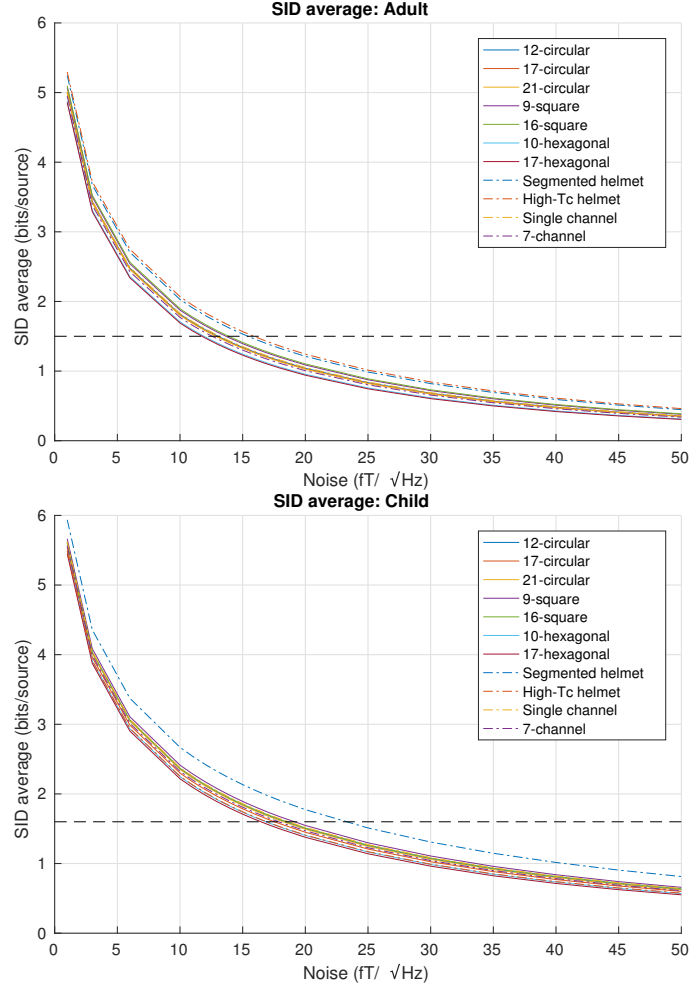
Figure 11: *The SID average over all sources as a function of the different noise levels. The first figure is the average SID values for the adult and the second figure is for the child, sampled for each layout.*

If we choose the optimistic noise level equal to $10\,\mathrm{fT}/\sqrt{\mathrm{Hz}}$, the SID average value for all the high-Tc simulations is higher than the Elekta system, i.e more spatial information is gained. But for the conservative choice of noise level $50\,\mathrm{fT}/\sqrt{\mathrm{Hz}}$, the Elekta system performs better than the high-Tc layouts. Seen in figure 11, the performance of different layouts varies between the two subjects. The ranking of the 6 best performing layouts when evaluating the SID average, from best to worst (evaluated from figure 11), can be seen below.

Adult:
1. high-Tc helmet
2. Segmented helmet
3. 16-channel square
4. 9-channel square
5. Single-channel
6. 12-channel circular

Child:
1. Segmented helmet
2. 9-channel square
3. Single-channel
4. 16-channel square
5. 12-channel circular
6. 21-channel circular

For the adult, the high-Tc helmet array gave the highest value of SID average, extracting 40% more spatial information per source than the Elekta system if the sensor noise level is set to the optimistic one. As

for the child, the segmented helmet gave the highest average SID, extracting 80% more than the Elekta system. Notice that the five chosen final layouts that performed the best when evaluating I_{tot} has a good SID average result as well for both subjects, seen in the tables above. As mentioned before, the high-Tc helmet performs well on the adult when evaluating both SID_{avg} and I_{tot}, but is worse for the child. The layout with the least gained spatial information was both the hexagonal shaped cryostat, for both subjects.

It is noteworthy that when evaluating I_{tot} in the previous chapter (figure 8 and 9), the result for the majority of the on-scalp layouts were better than the Elekta system with the conservative sensor noise level, whereas the SID_{avg} for the on-scalp is lower than the Elekta system for the same noise level. This is due to comparing two different metrics, where I_{tot} represent the summation of all signals generated inside the brain and the SID_{avg} represent the coupling of individual and independent sources.

The reason to study the SID average values over different noise levels is to be able to evaluate which sensor noise level is required on a particular layout to gain the same (or better) average spatial information density as the Elekta system.

4.3.2 SID-maps

Although all SID-maps were simulated for both subjects, in this subsection only the best performing layouts with regards to I_{tot} and SID_{avg} are presented. These layouts are segmented helmet, both of the square shaped cryostat (9-channel and 16-channel), and the 12-channel circular. The SID-maps from the commercial Elekta system are also presented for comparison. The SID maps for the other simulated layouts are found in Appendix A.

The color map represents the number of bits extracted at each source. The sensor noise level is set to the optimistic value of $10 \, \text{fT}/\sqrt{\text{Hz}}$ for all on-scalp layouts on both subjects, whereas the Elekta system has a fixed noise level equal to $3 \, \text{fT}/\sqrt{\text{Hz}}$. For the Elekta helmet, the back part of the subject's head is resting at the back of the helmet with the top part of the head as high as possible, as they would be in a typical MEG recording.
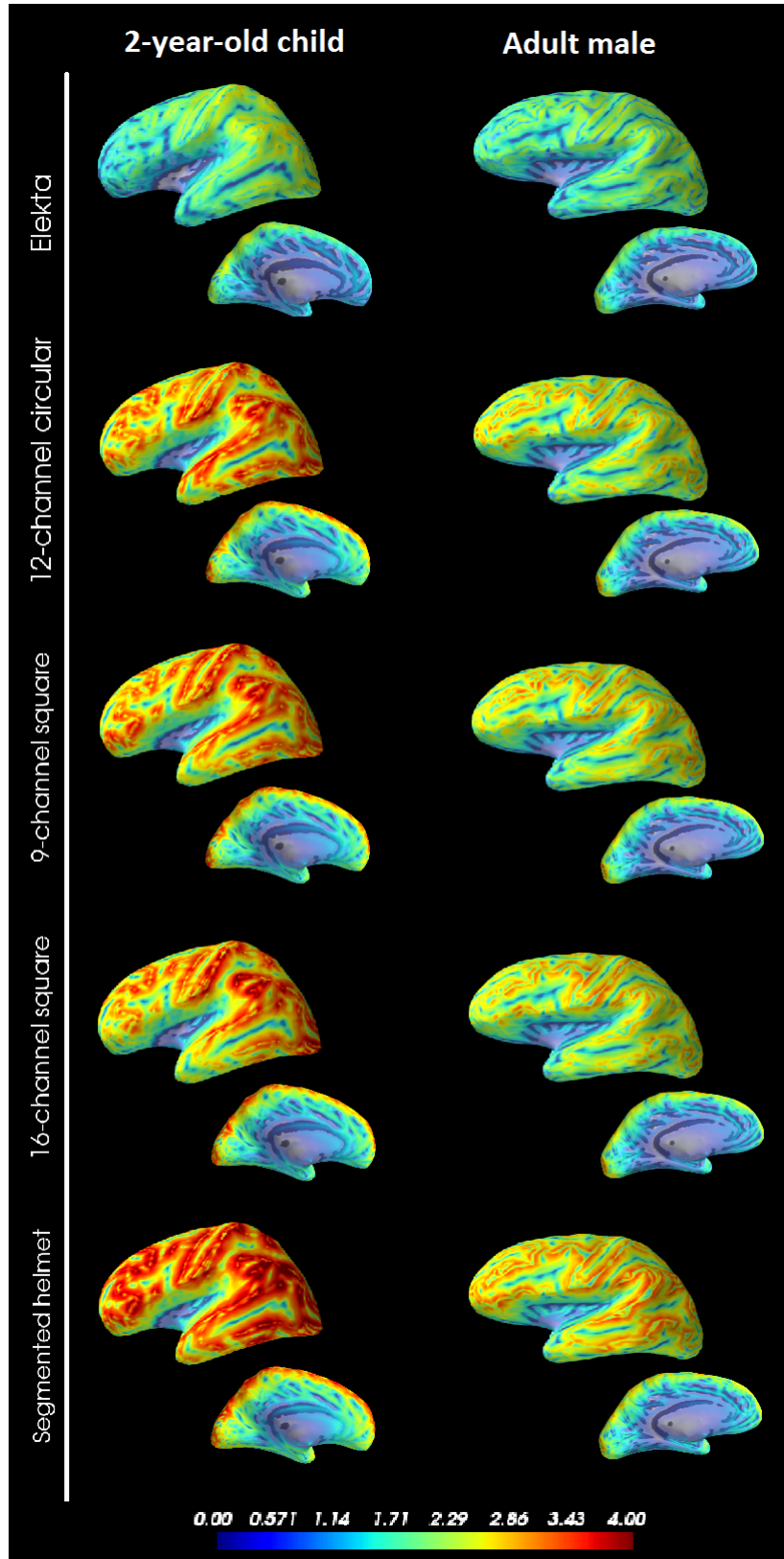
Figure 12: *SID-maps for selected layouts on a 2-year-old child (column 1) and an adult male (column 2)*

Comparing the result from the adult and the child, one can see that the overall SID values are higher for the child. This is as expected since the brain of a child is closer to the scalp's surface compared to the brain of an adult, which means that the SQUID sensors are closer to the source for children. Figure 12 shows the lateral and medial views of the left hemisphere for all MEG arrays sampled on both subjects, where the result do not differ significantly for the right hemisphere.

From looking at figure 12 it is clear that the on-scalp layouts outperform the commercial Elekta system by far when using the optimistic noise level. For the child case, the Elekta system shows uneven results comparing the frontal lobe (forehead) and the occipital lobe (back head), where the occipital lobe is much better sampled. Notice that there is a small difference in SID values comparing the frontal lobe to the occipital lobe for the on-scalp layouts sampled on the child as well, except for the segmented helmet where the recorded SID values are more evenly disturbed.

All the on-scalp layouts sampled on the adult show similar results. The frontal lobe and the occipital lobe have similar values for any one layout, and the SID maps are more evenly distributed for the adult as compared to the child. Looking closer at figure 12, one can see that the segmented helmet performs slightly better than the other layouts.

An increase in cryostat size may lead to SID-maps with larger patches of low coverage, since it will be more difficult to fit cryostats together. Since the segmented helmet uses 6 or 4 pieces densely covered with sensors, the overall coverage is improved, but the central scalp is potentially undersampled.

4.4   Additional subjects

After evaluating the result from I_{total}, SID_{avg} and the SID-maps of all the high-Tc layouts, the ones with the best results were evaluated on additional subjects to reinforce our previous result. The two new subjects are a 30-year-old female adult and another 2-year-old child. The simulations are done in exactly the same manner as for the previous subjects, the metrics I_{tot}, SID_{avg} and SID-maps use the same sensor noise levels and are presented the same as the previous chapters. The sensor placements of the four selected layouts can be seen in figure 13.
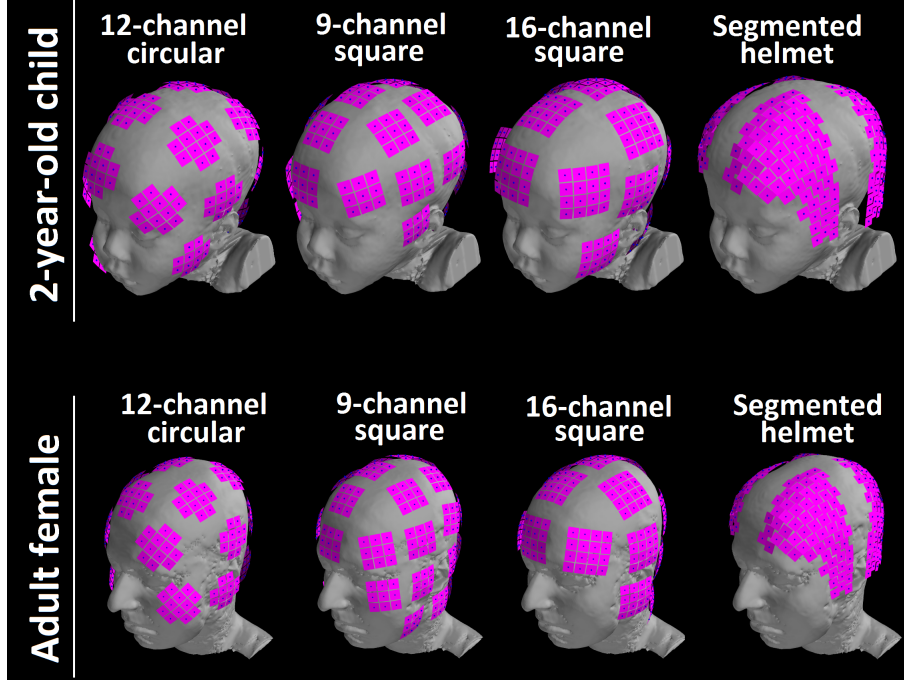
Figure 13: *The four selected layouts and their placements on the additional subjects.*

The summarized array parameters for the second adult (adult2) and child (child2) are shown below.

Table 5: *Parameters for each layout sampled on adult2 and child2.*

	Average standoff from scalp (mm)	Total number of sensors
	Female Adult/2-year-old Child	*Female Adult/2-year-old Child*
12-channel circular	2.7/2.7	240/240
9-channel square	2.3/2.3	297/243
16-channel square	3.3/3.4	320/288
Segmented helmet	4.6/6.6	324/324

Notice that the average standoff for the segmented helmet is quite large (especially for child2), which might detract from the results. But the number of sensors is largest for the segmented helmet as well so it is hard to know from these parameters which layout will perform the best. The middle part of the segmented helmet is excluded for both the new subjects due to its size.

The figures below represent the total information conveyed by the best on-scalp layouts, where the noise level is equal to the conservative one ($50\,\mathrm{fT}/\sqrt{\mathrm{Hz}}$).
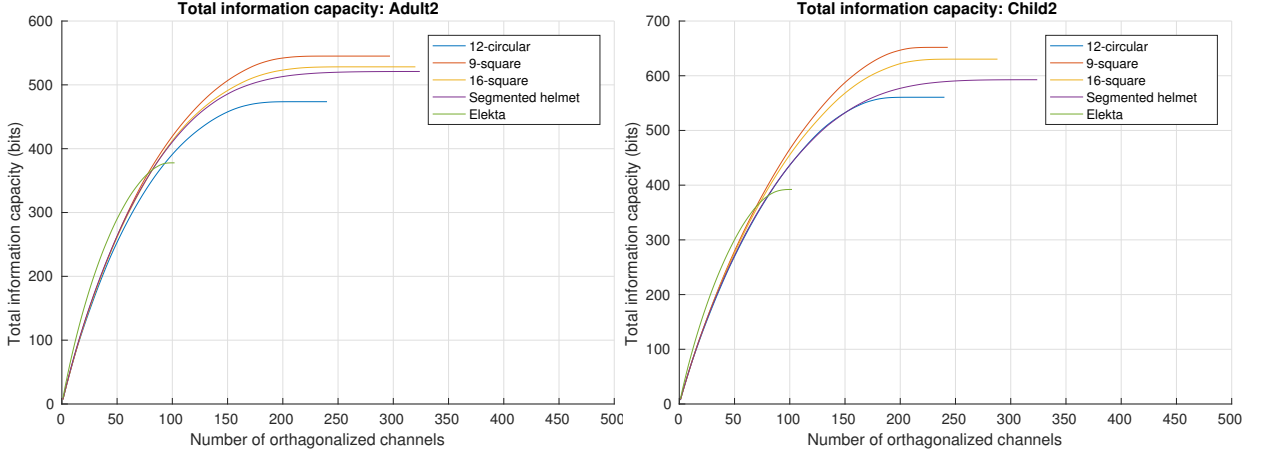
Figure 14: *Cumulative sum of total information capacity for all the selected layouts and the commercial Elekta system using the conservative noise level of $50 \, \text{fT}/\sqrt{\text{Hz}}$. The left figure shows the result for adult2 while the right figure shows the result for child2.*

Evaluation of I_{tot} in figure 14 shows that the square cryostats, 9-channel and 16-channel, performed the best followed by the segmented helmet and lastly the 12-channel circular, for both adult2 and child2. Comparing these result to the first child and adult, figures 8 and 9, the total information gained from each on-scalp layout has almost the same values ($\sim$450-750), except for the segmented helmet for the first child where I_{tot} is around 900). Notice that the Elekta helmet sampled on the two new subjects resulted in poor I_{tot}, below 400 bits, the same as for the first adult and child.

The table below shows maximal information conveyed from the source for both the conservative and the optimistic sensor noise level.

Table 6: *Maximal information capacity, all layouts sampled on the second adult and child for both the conservative and optimistic sensor noise level.*

	Adult2		**Child2**	
	$\sigma_{noise} = 50 \, \text{fT}/\sqrt{\text{Hz}}$	$\sigma_{noise} = 10 \, \text{fT}/\sqrt{\text{Hz}}$	$\sigma_{noise} = 50 \, \text{fT}/\sqrt{\text{Hz}}$	$\sigma_{noise} = 10 \, \text{fT}/\sqrt{\text{Hz}}$
12-channel circular	473.6	886.5	560.7	990.9
9-channel square	545.1	1014.2	651.9	1136.4
16-channel square	528.2	1010.8	630.3	1132.4
Segmented Helmet	521.0	1031.9	592.7	1145.4

The red marked digits in table 6 are the layouts that conveyed the most information for each case of subject and sensor noise level. If we choose the conservative noise level, the best performing layout is the square 9-channel, whereas if we choose the optimistic noise level, the segmented helmet gathered the most information. One can see that the worst performing layout is the 12-channel circular, for both noise levels and both subjects. As pointed out before, a reduced noise level leads to an increased performance for each individual sensor, meaning that denser layouts (i.e. the segmented helmet) benefit more than sparse ones.

The SID average is also evaluated for the two new subjects with the four top layouts. As before, the fixed average SID value of the Elekta system is represented by a reference line (black dashed line). For the Elekta helmet sampled on the two new subjects, the SID average value is 1.6 bits/source for both adult2 and child2.
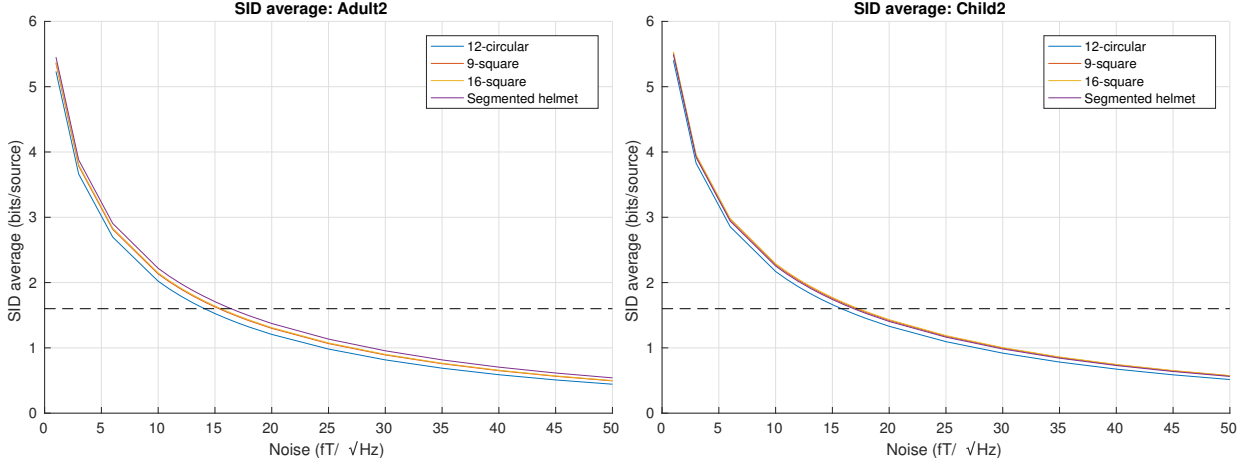
Figure 15: *The SID average over all sources as a function of the different noise levels. The left figure shows the average SID values for adult2 and the right figure is for child2, sampled for each layout.*

For adult2, the best performing layout when evaluating the SID average is the segmented helmet, which extract 40% more spatial information than the Elekta system for the optimistic noise level, followed by the square cryostats (first the 16-channel and then the 9-channel) and lastly the 12-channel circular. There is a slight difference for child2, where the best layouts are the square cryostats, first 16-channel that extracts 44% more information than the Elekta system for the optimistic sensor noise level, then 9-channel. After that comes the segmented helmet and lastly the 12-channel circular layout. Same as for the first adult and child, figure 11, the on-scalp layouts have a higher value than the Elekta system if the optimistic noise level is chosen, but for the conservative noise level Elekta has the higher SID average value.

As for the SID-maps, the sensor noise level is set to the optimistic one and the range has the same values as before, i.e when first adult and child was evaluated.
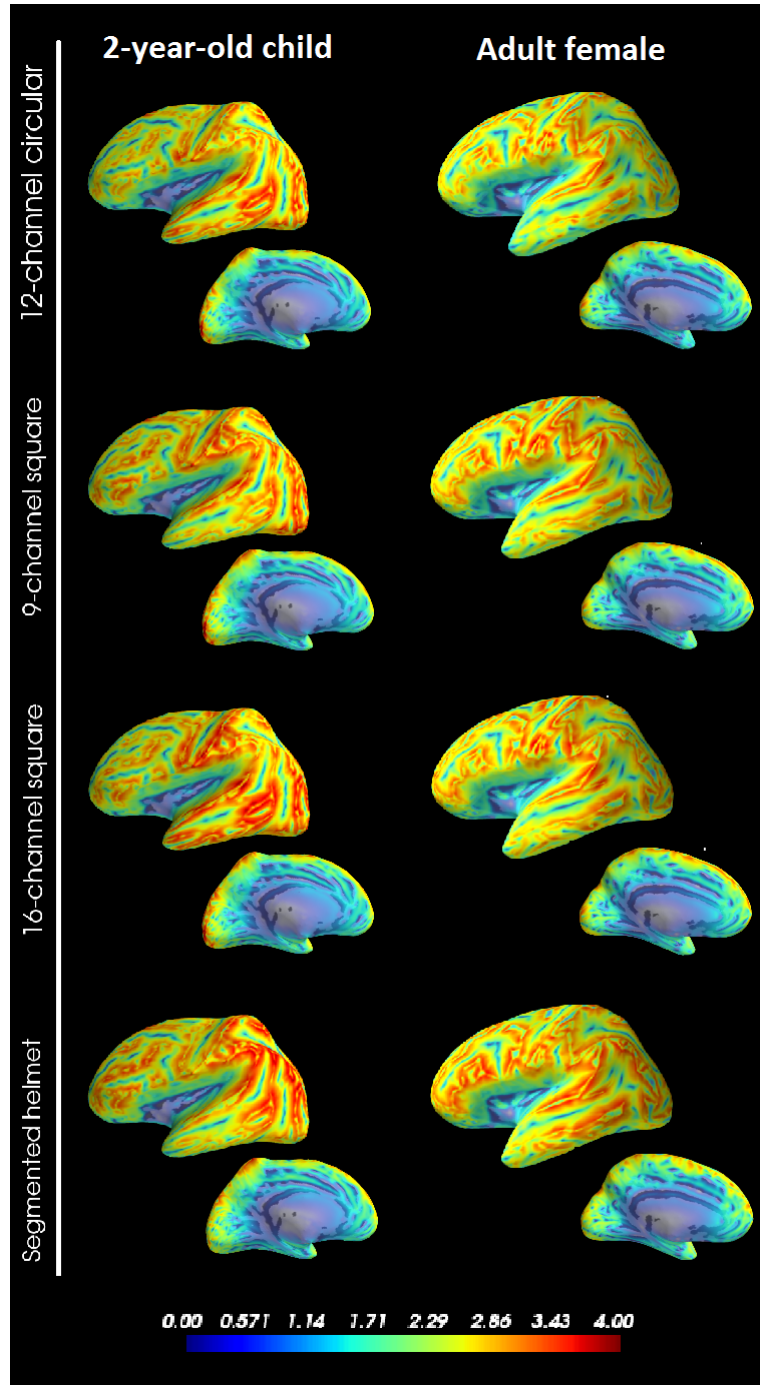
Figure 16: *SID-maps for selected layouts on the second 2-year-old child and the adult female*

The SID-maps for the second child in column 1, figure 16, has an unevenly distributed SID-map (similar to the first child) where the occipital lobe is sampled with more bits per source than the frontal lobe, for all the layouts. The 9-channel square layout has a more equally distributed SID-maps around the head. The smallest of the sampled SID-values was given by the 12-channel circular layout.

For the second adult, seen in column 2 figure 16, the SID-maps for all the on-scalp layouts are equally

distributed over the brain, the same as for the first adult. Overall the segmented helmet performed better than the other on-scalp layouts, and the layout with the least extracted bits per source was the 12-channel circular, again.

When evaluating all the metrics, i.e I_{tot}, SID_{avg} and SID-maps, the results from adult2 and child2 are similar to each other, compared to the big difference between the first adult and child. Seen in table 1, the parameters cortical surface area and number of sources are similar between adult2 and child2, whereas the difference between these parameters for the first adult and child are large. The female adult has a smaller head than the male adult, which is also the reason for excluding the middle parts of the segmented helmet.

5 Discussion

This section discussed the results found during the thesis as well as some areas for improvement.

5.1 Summary of the results

The aim of the thesis was to create and evaluate different configurations of realistic designs of on-scalp MEG sensor layouts, where these high-Tc layouts were compared to the commercial Elekta system. All the new high-Tc layouts we created were first simulated for two subjects: a 35-year-old adult (male) and a 2-year-old child. The reason for including the child is to be able to evaluate the adaptability of on-scalp MEG arrays. After evaluating our simulations based on the metrics I_{tot}, SID_{avg} and SID-maps, the four best were chosen to be simulated on two additional subjects for comparison: a 30-year-old female and another 2-year-old child.

In terms of total information capacity, almost all of the on-scalp arrays outperformed the commercial low-Tc Elekta system, even for the conservative noise level of $50\,\mathrm{fT}/\sqrt{\mathrm{Hz}}$. For this level, the best I_{tot} for the adult was the single-channel layout while for the child it was the segmented helmet. However, when using the optimistic noise level of $10\,\mathrm{fT}/\sqrt{\mathrm{Hz}}$, the segmented helmet had the highest I_{tot} for both primary subjects. This can be attributed to the reduction in noise level effectively increasing the range of each sensor. While the single-channel is perfectly on-scalp for every sensor location, the segmented helmet has a much denser array. If the sensors being used are noisier, a low average standoff is most important, whereas if there is less noise a more densely packed array performs better (such as the segmented helmet).

As for the SID average and the SID-maps, all the high-Tc arrays performed better than the Elekta system if the optimistic noise level was used. The layout that extracted the largest average SID for the adult is the high-Tc helmet, followed by the segmented helmet and then the 16-channel square. As for the child, the segmented helmet performed best, followed by the 9-channel square and thereafter the single channel layout. Looking at the SID-maps in figure 12, one can see that the segmented helmet clearly extracts more bits per source for the child, whereas for the adult, the SID-maps between the layouts are very similar.

The worst performing on-scalp layout was the hexagonally shaped cryostat (both 10-channel and 17-channel) when evaluating all the metrics used in the thesis. The overall performance of the circular cryostats are quite good (results approximately between the squares and the hexagonal), where the 12-channel had the best overall performance.

For both the secondary subjects, the layout with the highest I_{tot} was the 9-channel square for the conservative noise level and the segmented helmet for the optimistic noise level. As for the SID average, the layout to extract the most spatial information was the segmented helmet for adult2 and the 16-channel square layout for child2. Evaluating the SID-maps on child2 was difficult due to uneven sampling around the head, see figure 16. For example, the frontal areas of the brain were better sampled for the 9-channel square as compared to the 16-channel square, but the 16-channel square had better sampling at towards the back of the brain. As for adult2, the SID values are evenly distributed for all layouts with the segmented helmet extracting a bit more than the other designs, see figure 16 and figure 15.

5.2 Full head coverage vs Interest areas

The focus when placing each cryostat was to simply cover as much of the brain surface as possible. It seems fair to assume that this would be best when creating a system for any variety of diagnostic. The question is if there are any specific areas of the brain where coverage is always more essential, such as the visual cortex.

5.3 The segmented helmet - Adapting to general head sizes

The designs discussed in this thesis are only meant to be seen as proofs of concept. The segmented helmet layout is made to fit as tightly as possible to the 2-year-old child, assuming it to be among the smallest heads needed to measure. Middle segments are added for the male adult in order to increase total coverage. Applying it to subjects with different head-shapes highlights the need for more adaptability. As can be seen in figure 17, for the female subject there are large gaps between the back and front segments of the helmet, as well as between the two frontal segments. The middle segment used for the male subject did not quite fit for the female case, and so had to be omitted.

Figure 17: *Side-by-side comparison of the segmented helmet on the male and female adult subjects*

A possible fix for the circled frontal areas would be to add another pair of strips running front-to-back, to be inserted medially at the front and back of the head. However, when creating these strips other concerns need to be taken into account, see chapter 5.4. Relevant to these solutions are the differences between adults and children when it comes to thickness of the skull. A younger subject means a thinner layer between sensors and brain. This in turn leads to a lower stand-off per sensor. Therefore, if in a position where a compromise needs to be made for adult or child subjects regarding size it is advised to make it in favor of the adult case.

5.4 Cryostat walls

For all layouts, the single largest problem when reaching full coverage is empty space between sensor arrays caused by the cryostat walls. The problem is mitigated somewhat by using fewer, larger cryostats but will always remain an issue. This is easiest to observe in the case of the segmented helmet.

The total length of the adult subjects head from back to front is $\sim 210\,\text{mm}$. Each sensor is $11.5\,\text{mm}$, cryostat walls are $6\,\text{mm}$ of space outwards from each sensor. This means that adding a new cryostat requires a minimum of $6 \cdot 2 + 11.5 = 23.5\,\text{mm}$. Reducing the wall size, i.e improving insulation, would both increase general coverage and simplify creation of more adaptable layouts.

5.5 Choice of method - Practical parameters

The result above discusses the merits of different layouts in terms of SID-map coverage, SID-average and total information. In reality, there are many other factors to consider when designing a layout such as production method, the number of cryostats etc. For example, hexagonal cryostats will almost certainly be more difficult to produce than square or circular cryostats.

5.6 Applicability to other sensor technologies

Although in this report the calculations are done using high-Tc SQUIDs, there is no reason why similar methodology would not work for other sensor technologies such as OPMs. The parameters stand-off, sensor size, sensor location and noise together with concepts like packing problems will always be factors in designing any MEG sensor array. The additional constraints and allowances given by other sensor technology would of course need to be into account.

6   Conclusion

Designing a fully adaptable MEG sensor layout that is still viable performance-wise is a difficult task, and can be performed in any number of ways. If using a large amount of cryostats, a square shape is preferred, although a segmented helmet design was found to be most efficient.

Many other factors also impact performance, the most important of which are insulation size and noise level. Reducing these two parameters would significantly increase the viability of high-Tc MEG arrays as compared to low-Tc.

Further studies could be done into production methods and what constraints are set on design from that perspective.

References

[1] J. F. Schneiderman. Information content with low-vs. high-tc squid arrays in meg recordings: The case for high-tc squid-based meg. *Journal of Neuroscience Methods*, 222:42–46, 2014.

[2] Institue for learning and Brain Sciences. What is magnetoencephalography (MEG)?, April 2017. `http://ilabs.washington.edu/what-magnetoencephalography-meg`.

[3] S. P. Singh. Magnetoencephalography: Basic principles. *Annals of Indian Academy of Neurology*, 17:107–112, 2014. `https://www.ncbi.nlm.nih.gov/pmc/articles/PMC4001219/`.

[4] B. Riaz, C. Pfeiffer, and J. F. Schneiderman. Evaluation of realistic layouts for next generation on-scalp meg: spatial information density maps. Unpublished, 2017.

[5] E. Botoa, S. Meyerb, V. Shahc, O. Alemc, and S. Knappec et al. A new generation of magnetoen-cephalography: Room temperature measurements using optically-pumped magnetometers. *Elsevier: Neuroimage*, 149:404–414, 2017. `http://dx.doi.org/10.1016/j.neuroimage.2017.01.034`.

[6] A. Filler. The history, development and impact of computed imaging in neurological diagnosis and neurosurgery: CT, MRI, and DTI. *Nature Precedings*, 2009. `http://precedings.nature.com/documents/3267/version/5`.

[7] NIH Blueprint for Neuroscience Research. MEG and EEG | project components | human connectome project, 2017. `http://www.humanconnectome.org/about/project/MEG-and-EEG.html`.

[8] R. Hari and R. Salmelin. Magnetoencephalography: From SQUIDs to neuroscience: Neuroimage 20th anniversary special edition. *Elsevier: Neuroimage*, 61:386–396, 2011. `http://dx.doi.org/10.1016/j.neuroimage.2011.11.074`.

[9] K. Spring. Spatial resolution in digital images, 2012. `http://micro.magnet.fsu.edu/primer/java/digitalimaging/processing/spatialresolution/`.

[10] Y. Weerakkody and U. Bashir. Temporal resolution. `https://radiopaedia.org/articles/temporal-resolution`.

[11] M. Martin, K. Eid, and J. Catchmark. Fabricating superconducting quantum interference device, squid, nanostructures for single spin detec-tion. *Journal of Young Investigators*, 2007. `http://www.jyi.org/issue/fabricating-superconducting-quantum-interference-device-squid-nanostructures-for-single-spin-det`

[12] R. L. Fagaly. Superconducting quantum interference device instruments and applications. *Review of Scientific Instruments*, 77, 2006. `http://dx.doi.org/10.1063/1.2354545`.

[13] National Institute of Standards and USA Technology. Josephson effect. `http://www.supraconductivite.fr/en/index.php?p=applications-squid-josephson`.

[14] J. Clarke and A. Braginski. *The SQUID Handbook*. Wiley-VCH, Weinheim, 2006.

[15] J. E. T. Knuutila, A. Ahonen, M. S. Hämäläinen, M. J. Kajola, P. P. Laine, and O. V. Lounasmaa et al. A 122-channel whole-cortex squid system for measuring the brain's magnetic fields. *IEEE Transactions on Magnetics*, 29, 1993. `http://ieeexplore.ieee.org/document/281163/`.

[16] J. Haueisen. The influence of forward model conductivities on eeg/meg source reconstruction. *Non-invasive Functional Source Imaging of the Brain and Heart and the International Conference on Functional Biomedical Imaging*, 2007. `http://ieeexplore.ieee.org/document/4387676/`.

[17] F. Tadel, E. Bock, J. C. Mosher, R. Leahy, and S. Baillet. Head modeling. `http://neuroimage.usc.edu/brainstorm/Tutorials/HeadModel#Forward_model`.
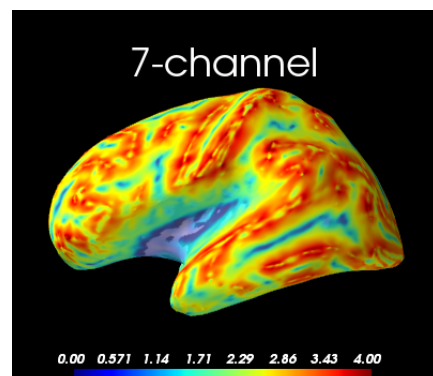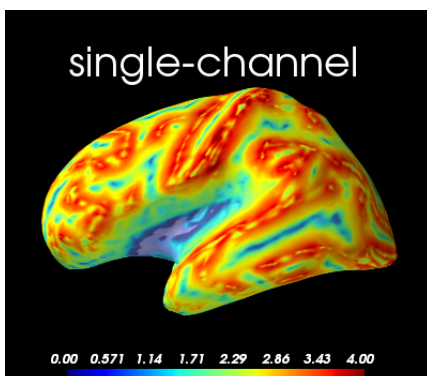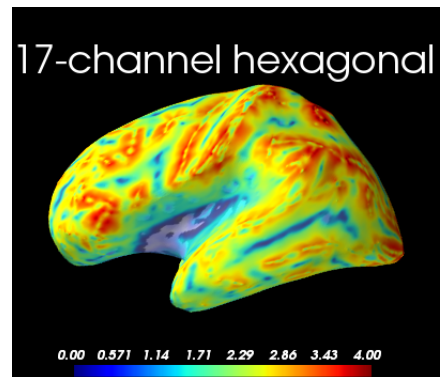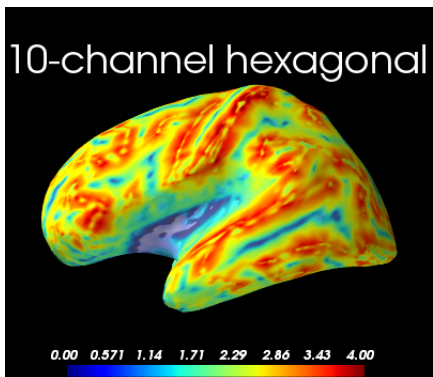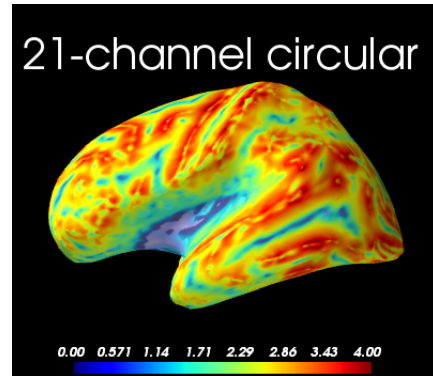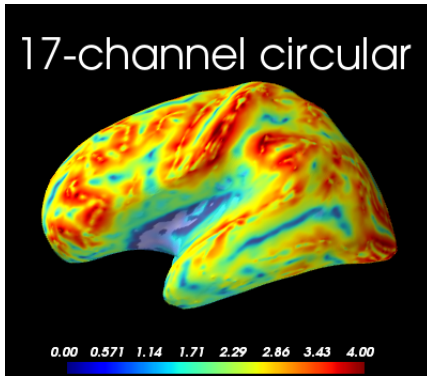
[18] P. K. Kemppainen and R. J. Ilmoniemi. Channel capacity of multichannel magnetometers. advances in biomagnetism. *US: Springer*, page 635–6388, 1990.

[19] M. S. Hämäläinen and R. J. Ilmoniemi. Interpreting magnetic-fields of the brain – minimum norm estimates. *Medical & Biological Engineering & Computing*, 32:35–42, 1994.

[20] J. Nenonen, M. Kajola, J. Simola, and A. Ahonen. Total information of multichannel meg sensor arrays. proceedings of the 14th international conference on biomagnetism. *Biomag2004*, page 630-631, 2004.

[21] J. Iivanainena, M. Stenroosa, and L. Parkkonena. Measuring meg closer to the brain: Performance of on-scalp sensor arrays. *Elsevier: Neuroimage*, 147:542–553, 2016. `https://doi.org/10.1101/073585`.

[22] F. Öisjöen, J. F. Schneiderman, G. A. Figueras, M. L. Chukharkin, A. Kalabukhov, A. Hedström, M. Elam, and D. Winkler. High-tc superconducting quantum interference device recordings of spontaneous brain activity: Towards high-tc magnetoencephalography. *Applied Physics Letters*, 100(132601), 2012.

[23] M. I. Faley, U. Poppe, K. Urban, D. N. Paulson, and R. L. Fagaly. A new generation of the hts multilayer dc-squid magnetometers and gradiometers. *Journal of physics: Conference Series*, 43:1199–1202, 2006.

[24] E. V. Popov. Geometric approach to chebyshev net generation along an arbitrary surface represented by NURBS. *International conference on computer graphics and vision Graphi-Con'2002*, 2002.
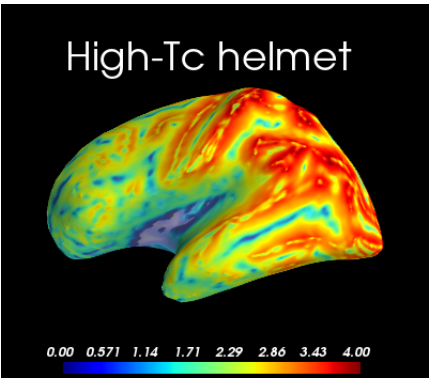
Appendix

A - SID maps of the remaining layouts

The layouts that were not presented in the result was: 17-circular, 21-circular, 10-hexagonal, 17-hexagonal, High-Tc helmet, Single channel and 7 channel.

The 2-year-old child

Adult male